DESY-0?-???
2nd July 2008

A measurement of the Q^2, W and t dependences of deeply virtual Compton scattering at HERA

ZEUS Collaboration

Abstract

Deeply virtual Compton scattering, $\gamma^\star p \rightarrow \gamma p$, has been measured in e^+p collisions at HERA with the ZEUS detector using an integrated luminosity of 61.1 pb $^{-1}$. Cross sections are presented as a function of the photon virtuality, Q^2, and photon-proton centre-of-mass energy, W, for a wide region of the phase space, $Q^2 > 1.5$ GeV^2 and $40 < W < 170$ GeV. A subsample of events in which the scattered proton is measured in the Leading Proton Spectrometer, corresponding to an integrated luminosity of 31.3 pb $^{-1}$, is used for the first direct measurement of the differential cross section as a function of t where t is the square of the four-momentum transfer at the proton vertex.

1 Introduction

This paper presents cross-section measurements for the exclusive production of a real photon in diffractive ep interactions, $ep \rightarrow e\gamma p$, a process known as deeply virtual Compton scattering (DVCS). In perturbative QCD, this process is described by the exchange of two partons, with different longitudinal and transverse momenta in a colourless configuration. At the $\gamma^* p$ centre-of-mass energies, W, available for ep collisions at the HERA collider, for large momentum-transfer squared at the lepton vertex, Q^2, the DVCS process is dominated by two-gluon exchange. Measurements of the DVCS cross section provide constraints on the generalised parton distributions (GPDs) [1–5], which carry information about the wave function of the proton. The transverse distribution of partons in the proton, which is not accessible through the measurements of the F_2 structure function, is accounted for the dependence of the GPDs on the four-momentum transfer squared at the proton vertex, t. The initial and final states of the DVCS process are identical to those of the purely electromagnetic Bethe-Heitler (BH) process. The interference between these two processes in principle provides information about the real and imaginary parts of the QCD scattering amplitude [6–8]. However, the interference is expected to be small in the kinematic region studied in this paper [6, 7].

The simplicity of the final state and the absence of complications due to hadronisation mean that the QCD predictions for DVCS are expected to be more reliable than for exclusive vector meson production [9–16], which has been extensively studied in ep collisions at HERA. Several measurements of DVCS at high W are available [17–20]. The analysis presented here extends the kinematic range of the previous ZEUS measurement [18] to $1.5 < Q^2 < 100\,\text{GeV}^2$ and $40 < W < 170\,\text{GeV}$. A subsample of the data in which the scattered proton is measured in the ZEUS leading proton spectrometer (LPS) [21] is used for the direct measurement of the t dependence of the DVCS cross section.

2 Experimental set-up

The data used for this measurement, corresponding to an integrated luminosity of $61.1\,\text{pb}^{-1}$, were taken with the ZEUS detector at the HERA ep collider in the years 1999 and 2000, when HERA collided positrons of energy 27.5 GeV with protons of energy 920 GeV. The subsample used to measure the t distribution was collected in 2000 and corresponds to an integrated luminosity of 31.3 pb^{-1}.

A detailed description of the ZEUS detector can be found elsewhere [22, 23]. A brief outline of the components most relevant for this analysis is given below.

Charged particles were tracked in the CTD [24]. It consisted of 72 cylindrical drift-chamber layers, organised in nine superlayers covering the polar-angle[1] region $15^\circ < \theta < 164^\circ$. The CTD operated in a magnetic field of 1.43 T provided by a thin solenoid. The transverse-momentum resolution for full-length tracks was $\sigma(p_T)/p_T = 0.0058 p_T \oplus 0.0065 \oplus 0.0014/p_T$, with p_T in GeV.

The uranium-scintillator calorimeter (CAL) [25] covered 99.7% of the total solid angle and consisted of three parts: the forward (FCAL), the barrel (BCAL) and the rear (RCAL) calorimeters. Each part was subdivided transversely into towers and longitudinally into one electromagnetic section (EMC) and either one (in RCAL) or two (in BCAL and FCAL) hadronic sections (HAC). The CAL energy resolutions, as measured under test-beam conditions, were $\sigma(E)/E = 0.18/\sqrt{E}$ for positrons and $\sigma(E)/E = 0.35/\sqrt{E}$ for hadrons, with E in GeV.

The position of positrons scattered at small angles to the positron-beam direction was determined combining the information from the CAL, the small-angle rear detector (SRTD) and the hadron-electron separator (HES) [26, 27].

The FPC [28] was used to measure the energy of particles in the pseudorapidity range $\eta \approx 4.0-5.0$. It consisted of a lead-scintillator sandwich calorimeter installed in the 20×20 cm^2 beam hole of the FCAL. The energy resolution as measured in a test beam, was $\sigma_E/E = (0.41 \pm 0.02)/\sqrt{E} \oplus 0.062 \pm 0.002$, with E in GeV, for positrons, and after combining information from FPC and FCAL, the resolution was $\sigma_E/E = (0.65 \pm 0.02)/\sqrt{E} \oplus 0.06 \pm 0.01$, with E in GeV, for pions and the e/h ratio was close to unity.

The LPS [21] detected positively charged particles scattered at small angles and carrying a substantial fraction, x_L, of the incoming proton momentum; these particles remained in the beam-pipe and their trajectory was measured by a system of silicon microstrip detectors that was inserted very close (typically whitin a distance of a few mm) to the proton beam. The detectors were grouped in six stations, S1 to S6, placed along the beam line in the direction of the proton beam, between 23.8 m and 90.0 m from the interaction point. The particle deflections induced by the magnets of the proton beam-line allowed a momentum analysis of the scattered proton. For the present measurements, only stations S4, S5 and S6 were used. The resolutions were about 0.5% on the longitudinal momentum fraction and about 5 MeV on the transverse momentum. The LPS acceptance was approximately 2% and x_L-independent for $x_L \gtrsim 0.98$; it increased smoothly to about 10% as x_L decreases to 0.9.

The luminosity was measured from the rate of the bremsstrahlung process $ep \to e\gamma p$, where the photon was measured in a lead-scintillator calorimeter [29] placed in the HERA tunnel at $Z = -107$ m.

3 Monte Carlo simulations

The acceptance and the detector response were determined using Monte Carlo (MC) simulations. The detector was simulated in detail using a program based on Geant 3.13 [30]. All of the simulated events were processed through the same reconstruction and analysis chain as the data.

A MC generator, GenDVCS [31], based on a model by Frankfurt, Freund and Strikman (FFS) [32], was used to simulate the elastic DVCS process. The ALLM97 [33] parameterisation of the F_2 structure function of the proton was used as input. The t dependence was assumed to be exponential with a slope parameter b set to 4.5 GeV^{-2}, independent of W and Q^2.

The elastic, $ep \rightarrow e\gamma p$, and inelastic $ep \rightarrow e\gamma Y$ BH processes, where Y is the hadronic final state, and the QED di-lepton production, $ep \rightarrow ee^+e^-p$, were simulated using the Grape-Compton[2] [34] and the Grape-Dilepton [34] generators. These two MC programs are based on the automatic system Grace [35] for calculating Feynman diagrams. A possible contribution from vector meson electroproduction was simulated by the ZEUSVM generator [36]. To account for electroweak radiative effects, all the generators were interfaced to Heracles 4.6 [37].

4 Kinematic variables and event selection

The process $ep \rightarrow e\gamma p$ is described by the following variables:

- $Q^2 = -q^2 = -(k - k')^2$, the negative four-momentum squared of the virtual photon, where k (k') is the four-momentum of the incident (scattered) positron;
- $W^2 = (q + p)^2$, the squared centre-of-mass energy of the photon-proton system, where p is the four-momentum of the incident proton;
- $x_L = \frac{p' \cdot k}{p \cdot k}$, the fractional energy of the outgoing proton, where p (p') are the four-momentum of the incident (scattered) proton;
- $t = (p - p')^2$, the squared four-momentum transfer at the proton vertex.

For the Q^2 range of this analysis, $Q^2 > 1.5$ GeV^2, and at small values of t, the signature of DVCS and BH events consists of a scattered positron, a photon and a scattered proton. The scattered positron is observed in the RCAL, and the photon in the RCAL or in the BCAL. The scattered proton remains in the beam pipe and, for a subsample of events, is detected in the LPS (LPS sample).

[2] Hereafter, the Grape-Compton generator is referred to as Grape.

The events were selected online via a three-level trigger system [22, 38]. The trigger required events with two isolated electromagnetic (EM) clusters with energy greater than 2 GeV. Offline, events were selected requiring two EM clusters as found by a dedicated, neural-network based, positron finder [39]. One cluster was required to be in the RCAL with energy $E_1 > 10\,\mathrm{GeV}$. Another cluster had to have a polar angle $\theta_2 < 2.85\,\mathrm{rad}$ and was required to be either in the RCAL, with energy $E_2 > 3\,\mathrm{GeV}$, or in the BCAL, with energy $E_2 > 2.5\,\mathrm{GeV}$. The angular range of the second cluster corresponds to the region of high reconstruction efficiency for tracks in the CTD. This requirement permits to identify the second EM cluster as originating from a photon or from a positron. For events with one track, a match was required between the track and one of the two EM clusters. Events with more than one track were rejected.

The condition $40 < E - P_Z < 70$ GeV was imposed, with $E = E_1 + E_2$ and $P_Z = E_1 \cos\theta_1 + E_2 \cos\theta_2$. This requirement rejected photoproduction events and also events in which a hard photon was radiated from the incoming positron.

After this selection, the two EM clusters were ordered such that $E_1 > E_2$, which results in $\theta_1 > \theta_2$ due to kinematics. In the following, the two clusters will be denoted as EM1 and EM2, respectively.

Events with CAL energy deposits not associated with the two EM clusters were rejected if their energy was above noise-level [40]. In addition, the total energies measured in the FPC and in the FCAL were each required to be below 1 GeV. These elasticity requirements also suppress DVCS events and inelastic BH events in which the proton dissociates into a large mass system.

The sample was still contaminated by events in which a forward, low-mass hadronic system was not visible in the main detector. Alternatively a clean sample of elastic DVCS and BH events was obtained by additionally requiring the proton to be detected in the LPS.

For the purposes of this analysis, the values of Q^2 and W were determined for each event, independently of its topology, under the assumption that the EM1 cluster is the scattered positron. This assumption is always valid for DVCS events for the Q^2 range considered here. The electron method was used to determine Q^2 and the double-angle method to determine W [41].

To select DVCS and BH events with a scattered proton, a track candidate in the LPS was required. The event was rejected if, at any point, the distance of the track to the beam pipe was less than 0.04 cm. It was also rejected if the X position of the track impact point at station S4 was smaller than -3.3 cm. These cuts reduce the sensitivity of the acceptance on the uncertainty in the position of the beam-pipe apertures. To suppress background from overlays of the ep collisions with protons originating from beam-halo it was requested that $(E + P_Z) + 2p_Z^{\mathrm{LPS}} < 1865$ GeV, where p_Z^{LPS} is the longitudinal momentum of the scattered proton. The variable x_L was required to be within the range $0.96 < x_L < 1.02$ to exclude non-elastic events. The variable t was required to be in the range where the LPS acceptance was not small or rapidly changing. The kinematic region was $40 < W < 170\,\mathrm{GeV}$, $1.5 < Q^2 < 100\,\mathrm{GeV}^2$ and, for the LPS sample, $0.08 < |t| < 0.53\ \mathrm{GeV}^2$.

5 Background study and signal extraction

The selected events were subdivided into three samples, one in which there was no track associated with the EM2 cluster, γ sample, a second in which the track associated with EM2 had the same charge as the beam lepton, e sample, and a third in which the track associated with EM2 had the opposite charge to that of the beam lepton, wrong-sign-e sample. In more detail, the various sample have the following properties:

- γ sample: EM2, with no track pointing to it, is taken to be the photon and EM1 is assumed to be the scattered positron. Both BH and DVCS processes contribute to this topology. The sample consisted of 7618 events and 55 events after the LPS selection.
- e sample: EM2, with the positive-charge track pointing to it, is assumed to be the scattered-positron and EM1 is the photon. The sample is dominated by BH events. The number of DVCS events is predicted to be negligible due to the large Q^2 implied by the large positron scattering angle. This sample consisted of 11988 events and 33 events after the LPS selection.
- wrong-sign-e sample: EM2, with the wrong-charge-sign track pointing to it, may have originated from an e^+e^- final state accompanying the scattered positron, where one of the positrons escaped detection. This sample is dominated by non-resonant e^+e^- production and by J/ψ production and subsequent decay into e^+e^- and was used to study these background sources. The diffractive electroproduction of ρ, ω and ϕ mesons was found to be negligible. This sample consisted of 764 events and only one event after the LPS selection.

In the kinematic region of this analysis, the contribution of the interference term between the DVCS and BH amplitudes is very small when the cross section is integrated over the angle between the e and p scattering planes [6, 7]. Thus the cross section for exclusive production of real photons may be treated as a simple sum over the contributions from the DVCS and BH processes. The contribution of the latter can, therefore, be subtracted and the DVCS cross section determined.

The BH contribution to be subtracted was determined using the e sample which consists of elastic and inelastic BH events and a small fraction of exclusive e^+e^- production. The exclusive e^+e^- contribution was estimate with the wrong-sign-e to be $(5.6 \pm 0.3)\%$ and subtracted from the e sample.

The inelastic fraction of the BH events was estimated from the difference in the azimuthal angles, $\Delta\phi$, between the two electromagnetic clusters in the e sample. It was determined to be $(16 \pm 1)\%$ and was negligible in the LPS tagged subsample.

The cross section of the BH process measured in the data is $(4 \pm 1)\%$ smaller than the expectations of the GRAPE program (a detailed discussion can be found in [42, 43]). The GRAPE cross section was modified accordingly.

The DVCS distributions were obtained from the γ-sample by statistical subtraction of the BH contribution. The size of this contribution was determined by GRAPE and found to be $(56 \pm 1)\%$ for the untagged and $(21 \pm 3)\%$ for the LPS tagged sample.

The W and Q^2 distributions in the inclusive sample and the x_L and t distributions in the LPS sample, separately for the e sample, the γ sample and for the γ sample after BH background subtraction, are shown in Fig. 1. Also shown in the figure are MC expectations which describe well the data, whenever appropriate.

6 Systematic uncertainties

The uncertainties due to the reconstruction of the scattered positron and to the background subtraction were evaluate varying the selection criteria as follow:

- restricting the $E - P_Z$ to $45 < E - P_Z < 65$ GeV;
- shifting the reconstructed position of the electron with respect to the MC by $\pm$1mm;
- changing the elasticity requirements by $\pm$30 MeV in the EMC and $\pm$50 MeV in the HAC sections;
- varying the inelastic BH fraction by $\pm$1%.

Each individual systematic uncertainty affects single bins in Q^2 and W typically by less than 5% and by less than 10% in almost all cases. A single shift of more than 10% was observed in the highest Q^2 bin where statistical fluctuations dominate.

To evaluate the uncertainties due to the reconstruction of the final-state proton,

- the cut on the minimum distance to the beam-pipe was increased to 0.1 cm;
- the t range was tigthened to $0.1 < |t| < 0.5$ GeV^2;
- the kinematic limit of the beam-halo background cut was lowered to 1855 GeV;
- the x position of the track impact point at station S4 was restricted to -32 mm.

The total systematic uncertainty was found to be $\pm 8\%$ and smaller than the statistical uncertainty. The total systematic uncertainty was obtained by adding in quadrature the individual contributions.

For the LPS data, the quoted uncertainties do not include an overall normalisation uncertainty of $\pm 7\%$ which originates mostly from the uncertainty on the simulation of the proton-beam optics. This uncertainty can be treated as a normalisation uncertainty as it is largely independent of the kinematic variables and are not included in the figures.

The uncertainty in the determination of the integrated luminosity of $\pm 2.25\%$ and on the proton dissiation bachground of 1.3% is not included in the figures.

7 Cross-section determination and results

The $\gamma^* p$ cross section of the DVCS process was evaluated as a function of W, Q^2 and t using the expression

$$\sigma^{\gamma^* p \to \gamma p}(W_i, Q_i^2) = \frac{(N_i^{\mathrm{obs}} - N_i^{\mathrm{BH}}) \cdot (1 - f_{p-\mathrm{diss}})}{N_i^{\mathrm{MC}}} \cdot \sigma^{\mathrm{FFS}(\gamma^* \mathrm{p} \to \gamma \mathrm{p})}(W_i, Q_i^2),$$

where N_i^{obs} is the total number of data events in the γ sample in bin i of W and Q^2, N_i^{BH} denotes the number of elastic and inelastic BH events in the γ sample in the bin, and N_i^{MC} is the number of events expected in the γ sample from GenDVCS for the luminosity of the data. The parameter $f_{p-\mathrm{diss}}$ is the fraction of the DVCS events in which the proton dissociated in a low-mass state. Its value was taken from previous pibblications [18, 44], $f_{p-\mathrm{diss}} = 17.5 \pm 1.3^{+3.7}_{-3.2}$. The cross section as predicted by the FFS model is denoted $\sigma^{\mathrm{FFS}}(\gamma^* p \to \gamma p)$ and was evaluated at the centre (W_i, Q_i^2) of each Q^2 and W bin. The differential cross section as a function of t was calculated from the LPS tagged sample for which $f_{\mathrm{p-diss}} = 0$. All the results are listed in tables 1 - 4.

The $\gamma^* p$ DVCS cross section, $\sigma^{\gamma^* p \to \gamma p}$, is presented in Fig. 2 as a function of Q^2 at $W = 104$ GeV and as a function of W at $Q^2 = 3.2$ GeV^2. The cross section shows a fast decrease with Q^2. A fit to the Q^2 dependence of the cross section, assuming the functional form $\sigma^{\gamma^* p \to \gamma p}(Q^2) \sim Q^{-2n}$, was performed for $W = 104$ GeV yielding $n = 1.54 \pm 0.05(\mathrm{stat.})$, smaller expexted for a pure propagator term [32]. The result is in agreement with other DVCS measurements at HERA at lower W [17–20]. As expected for DVCS [32], the decrease of the cross section with Q^2 is slower than for exclusive vector meson production [12–16, 45].

The cross section increases with W. In pQCD-based models, this behaviour is related to the increase of the gluon content of the proton with decreasing Bjorken-x. A fit to the

W dependence of the cross section, assuming a functional form $\sigma^{\gamma^* p\to\gamma p}(W) \sim W^\delta$, was performed for $Q^2 = 3.2$ GeV^2, yielding $\delta = 0.52 \pm 0.09$(stat.). The result in the extended region of W and at lower Q^2 with respect to the previous HERA results is in agreement with other measurements [17–20]. A second fit restricted to the region $1.5 < Q^2 < 5$ GeV^2 with average $Q^2 = 2.4$ GeV^2, was also performed leading to $\delta = 0.44 \pm 0.19$(stat.). The fit is presented in Fig. 3. Also shown in the figure are previous ZEUS measurements [18] and their extension to higher W values from the present analysis. The corresponding δ values fitted in a extended W range are given in the figure. Within the present accuracy the results do not show evidence of a Q^2 dependence of δ. This result is similar to that obtained for the exclusive production of J/ψ mesons [12–14, 45].

The first direct measurement of the $d\sigma^{\gamma^* p\to\gamma p}/dt$, extracted from the LPS-tagged events for an average $Q^2 = 3.2$ GeV^2 and an average $W = 104$ GeV, is shown in Fig. 4. The value of the slope parameter b extracted from an exponential fit to the differential cross section, $d\sigma^{ep\to e\gamma p}/dt \propto e^{-b|t|}$, is $b = 4.5 \pm 1.3$(stat.) ± 0.4(syst.) GeV^{-2} (χ^2/ndf $= 0.90$). This value is consistent with the results obtained by H1 [20] $b = 5.45 \pm 0.19$(stat.)± 0.34(syst.) GeV^{-2} at $Q^2 = 8$ GeV^2 and $W = 82$ GeV, from the transverse-momentum distribution of the photon candidate.

A compilation of b values as measured for various exclusive processes, including the result of this paper, is shown in Fig. 5 as a function of $Q^2 + M^2$, where M is the mass of the exclusive final state. The measured b values of DVCS tend to be lower but consistent with the corresponding values for vector mesons at similar scales. The fast rise of the DVCS cross section with W at $Q^2 = 2.4$ GeV^2 and the low value of b at $Q^2 = 3.2$ GeV^2 indicate that the DVCS process is a hard process even at low Q^2 scales.

8 Summary

The DVCS cross section has been measured as a function of Q^2 and W in the region $1.5 < Q^2 < 100$ GeV^2 and $40 < W < 170$ GeV. The measured cross section decreases steeply with Q^2, showing a dependence Q^{-2n}, with $n = 1.54 \pm 0.05$(stat.). The W cross section, rises with increasing W following a functional form W^δ, with $\delta = 0.52 \pm 0.09$(stat.), with little Q^2 dependence.

For the first time, the DVCS differential cross section as a function of t was measured by directly tagging the scattered proton. An exponential behaviour was assumed and a slope parameter $b = 4.5 \pm 1.3$(stat.) ± 0.4(syst.) GeV^{-2} was obtained from a fit at an average $Q^2 = 3.2$ GeV^2 and $W = 104$ GeV.

Acknowledgements

We thank the DESY Directorate for their support and encouragement. We are grateful for the support of the DESY computing and network services. We are specially grateful to the HERA machine group: collaboration with them was crucial to the successful installation and operation of the leading proton spectrometer. The design, construction and installation of the ZEUS detector were made possible by the ingenuity and effort of many people who are not listed as authors.

References

[1] M. Diehl, T. Gousset, B. Pire and J. Ralston, Phys. Lett. **B 411**, 193 (1997).

[2] M. Burkardt, Int. J. Mod. Phys. **A 18**, 173 (2003).

[3] M. Diehl, Eur. Phys. J. **C 25**, 223 (2002).

[4] V. Guzey and T. Teckentrup, Phys. Rev. **D 74**, 54027 (2006).

[5] K. Kumerički, Nucl. Phys. **B 794**, 223 (2008).

[6] L. Frankfurt, A. Freund and M. Strikman, Phys. Lett. **B 460**, 417 (1999).

[7] A.V. Belitsky, D. Müller and A. Kirchner, Nucl. Phys. **B 629**, 323 (2002).

[8] A. Freund and M. McDermott, Phys. Rev. **D65**, 091901 (2002).

[9] ZEUS Coll., J. Breitweg et al., Phys. Lett. **B 487**, 273 (2000).

[10] ZEUS Coll., S. Chekanov et al., Nucl. Phys. **B 718**, 2 (2005).

[11] ZEUS Coll., S. Chekanov et al., Nucl. Phys. **B 695**, 3 (2004).

[12] ZEUS Coll., J. Breitweg et al., Eur. Phys. J. **C 14**, 213 (2000).

[13] H1 Coll., C. Adloff et al., Phys. Lett. **B 483**, 360 (2000).

[14] ZEUS Coll., S. Chekanov et al., PMC Phys. **A**, 1 (2007).

[15] H1 Coll., A. Aktas et al., Eur. Phys. J. **C 46**, 585 (2006).

[16] H1 Coll., C. Adloff et al., Eur. Phys. J. **C 13**, 371 (2000).

[17] H1 Coll., C. Adloff et al., Phys. Lett. **B 517**, 47 (2001).

[18] ZEUS Coll., S. Chekanov et al., Phys. Lett. **B 573**, 46 (2003).

[19] H1 Coll., A. Aktas et al., Eur. Phys. J. **C 44**, 1 (2005).

[20] H1 Coll., F.D. Aaron et al., Phys. Lett. **B 659**, 796 (2008).

[21] ZEUS Coll., M. Derrick et al., Z. Phys. **C 73**, 253 (1997).

[22] ZEUS Coll., U. Holm (ed.), *The ZEUS Detector*. Status Report (unpublished), DESY (1993), available on `http://www-zeus.desy.de/bluebook/bluebook.html`.

[23] ZEUS Coll., M. Derrick et al., Phys. Lett. **B 293**, 465 (1992).

[24] N. Harnew et al., Nucl. Inst. Meth. **A 279**, 290 (1989);
B. Foster et al., Nucl. Phys. Proc. Suppl. **B 32**, 181 (1993);
B. Foster et al., Nucl. Inst. Meth. **A 338**, 254 (1994).

[25] M. Derrick et al., Nucl. Inst. Meth. **A 309**, 77 (1991);
A. Andresen et al., Nucl. Inst. Meth. **A 309**, 101 (1991);

A. Caldwell et al., Nucl. Inst. Meth. **A 321**, 356 (1992);
A. Bernstein et al., Nucl. Inst. Meth. **A 336**, 23 (1993).

[26] A. Bamberger et al., Nucl. Inst. Meth. **A 401**, 63 (1997).

[27] A. Dwurazny et al., Nucl. Inst. Meth. **A 277**, 176 (1989).

[28] ZEUS Coll., FPC group, A. Bamberger et al., Nucl. Inst. Meth. **A 450**, 235 (2000).

[29] J. Andruszków et al., Preprint DESY-92-066, DESY, 1992;
ZEUS Coll., M. Derrick et al., Z. Phys. **C 63**, 391 (1994);
J. Andruszków et al., Acta Phys. Pol. **B 32**, 2025 (2001).

[30] R. Brun et al., *GEANT3.* Technical Report CERN-DD/EE/84-1,CERN, 1987.

[31] P.R.B. Saull, *A Monte Carlo Generator for Deeply Virtual Compton Scattering at HERA*, 1999, available on `http://www-zeus.desy.de/physics/diff/pub/MC`.

[32] L.L. Frankfurt, A. Freund and M. Strikman, Phys. Rev. **D 58**, 114001 (1998). Erratum-ibid **D59** (1999) 119901.

[33] H. Abramowicz and A. Levy, Preprint DESY-97-251 (hep-ph/9712415), DESY, 1997.

[34] T. Abe, Comp. Phys. Comm. **136**, 126 (2001).

[35] T. Ishikawa et al., *GRACE manual: Automatic generation of tree amplitudes in Standard Models: Version 1.0.* KEK Report 92-19, 1993.

[36] K. Muchorowski, Ph.D. Thesis, Warsaw University, 1998 (unpublished).

[37] H. Spiesberger, *An Event Generator for ep Interactions at HERA Including Radiative Processes (Version 4.6)*, 1996, available on `http://www.desy.de/~hspiesb/heracles.html`.

[38] W.H. Smith, K. Tokushuku and L.W. Wiggers, *Proc. Computing in High-Energy Physics (CHEP),* Annecy, France, Sept. 1992, C. Verkerk and W. Wojcik (eds.), p. 222, CERN, Geneva, Switzerland (1992). Also in preprint DESY 92-150B.

[39] H. Abramowicz, A. Caldwell and R. Sinkus, Nucl. Inst. Meth. **A 365**, 508 (1995);
R. Sinkus and T. Voss, Nucl. Inst. Meth. **A 391**, 360 (1997).

[40] R. Ciesielski, *Exclusive J/Psi Production in Deep Inelastic ep Scattering in the ZEUS exeriment at HERA.* Ph.D. Thesis, Warsaw University, Warsaw, Poland, 2004.

[41] S. Bentvelsen, J. Engelen and P. Kooijman, *Proc. Workshop on Physics at HERA*, W. Buchmüller and G. Ingelman (eds.), Vol. 1, p. 23, Hamburg, Germany, DESY (1992);
K.C. Höger, ibid, p.43.

[42] I. Grabowska-Bołd, *Measurement of Deeply Virtual Compton Scattering Using the ZEUS Detector at HERA*. Ph.D. Thesis, University of Mining and Metallurgy, Cracow, Poland, Report DESY-THESIS-2004-034, 2003.

[43] S. Fazio, *Measurement of Deeply Virtual Compton Scattering cross sections at HERA and a new model for the DVCS amplitude*. Ph.D. Thesis, Calabria University, Rende (Cosenza), Italy, 2007, available on `http://www-zeus.desy.de/physics/diff/pub/theses.html`.

[44] ZEUS Coll., S. Chekanov et al., Eur. Phys. J. **C 24**, 345 (2002).

[45] ZEUS Coll., J. Breitweg et al., Eur. Phys. J. **C 6**, 603 (1999).

$\sigma^{\gamma^* p \to \gamma p}$		
Q^2 range (GeV^2)	Q^2 (GeV^2)	$\sigma^{\gamma^* p \to \gamma p}$ (nb)
1.5 - 5	3.25	$21.28 \pm 0.92^{+1.02}_{-1.29}$
5 - 10	7.5	$5.87 \pm 0.42^{+0.14}_{-0.30}$
10 - 15	12.5	$3.27 \pm 0.33^{+0.07}_{-0.16}$
15 - 25	20	$1.23 \pm 0.21^{+0.05}_{-0.08}$
25 - 40	32.5	$0.55 \pm 0.18^{+0.04}_{-0.04}$
40 - 100	70	$0.16 \pm 0.07^{+0.02}_{-0.02}$

Table 1: *The DVCS cross section, $\sigma^{\gamma^* p \to \gamma p}$, as a function of Q^2. Values are quoted at the centre of each Q^2 bin and at $W = 104$ GeV. The first uncertainty is statistical and the second systematic.*

$\sigma^{\gamma^* p \to \gamma p}$		
W range (GeV)	W (GeV)	$\sigma^{\gamma^* p \to \gamma p}$ (nb)
40 - 60	50	$14.47 \pm 1.05^{+0.20}_{-0.66}$
60 - 80	70	$20.38 \pm 1.57^{+0.61}_{-1.29}$
80 - 100	90	$17.95 \pm 1.35^{+0.64}_{-0.92}$
100 - 120	110	$20.65 \pm 1.26^{+0.59}_{-1.05}$
120 - 140	130	$26.42 \pm 1.84^{+0.78}_{-0.86}$
140 - 170	155	$27.60 \pm 3.74^{+1.99}_{-3.34}$

Table 2: *The DVCS cross section, $\sigma^{\gamma^* p \to \gamma p}$, as a function of W. Values are quoted at the centre of each W bin and for $Q^2 = 3.2$ GeV^2. The first uncertainty is statistical and the second systematic.*

$\sigma^{\gamma^* p \to \gamma p}$					
W range (GeV)	W (GeV)	$\sigma^{\gamma^* p \to \gamma p}$ (nb) $Q^2 = 2.4$ GeV^2	$\sigma^{\gamma^* p \to \gamma p}$ (nb) $Q^2 = 6.2$ GeV^2	$\sigma^{\gamma^* p \to \gamma p}$ (nb) $Q^2 = 9.9$ GeV^2	$\sigma^{\gamma^* p \to \gamma p}$ (nb) $Q^2 = 18.0$ GeV^2
40 - 65	52.5	$27.06 \pm 3.44^{+1.86}_{-0.59}$			
65 - 90	77.5	$22.36 \pm 3.11^{+3.23}_{-1.03}$			
90 - 115	102.5	$26.49 \pm 1.89^{+0.89}_{-0.95}$			
115 - 140	127.5	$35.94 \pm 2.63^{+1.72}_{-1.80}$			
140 - 170	155	$35.72 \pm 9.47^{+2.89}_{-2.94}$	$16.93 \pm 2.43^{+1.37}_{-1.40}$	$6.15 \pm 1.67^{+0.50}_{-0.51}$	$2.21 \pm 0.82^{+0.18}_{-0.18}$

Table 3: *The DVCS cross section, $\sigma^{\gamma^* p \to \gamma p}$, as a function of W in four Q^2 ranges. Values are quoted at the centre of each W bin and for the Q^2 values listed. The first uncertainty is statistical and the second systematic.*

$d\sigma^{\gamma^* p\to\gamma p}/dt$		
t range (GeV^2)	t (GeV^2)	$\sigma^{\gamma^* p\to\gamma p}/dt$ (nb/GeV^2)
0.08 - 0.19	0.14	34.6±9.6±10.0
0.19 - 0.31	0.25	32.7±9.4± 9.8
0.31 - 0.42	0.36	19.6±7.5± 7.7
0.42 - 0.53	0.47	5.7 ±4.1± 4.2

Table 4: *The DVCS differential cross section, $d\sigma^{\gamma^* p\to\gamma p}/dt$, as a function of $|t|$. Values are quoted at the centre of each $|t|$ bin and for $Q^2 = 3.2\,GeV^2$ and $W = 104\,GeV$. The first uncertainty is statistical and the second systematic.*

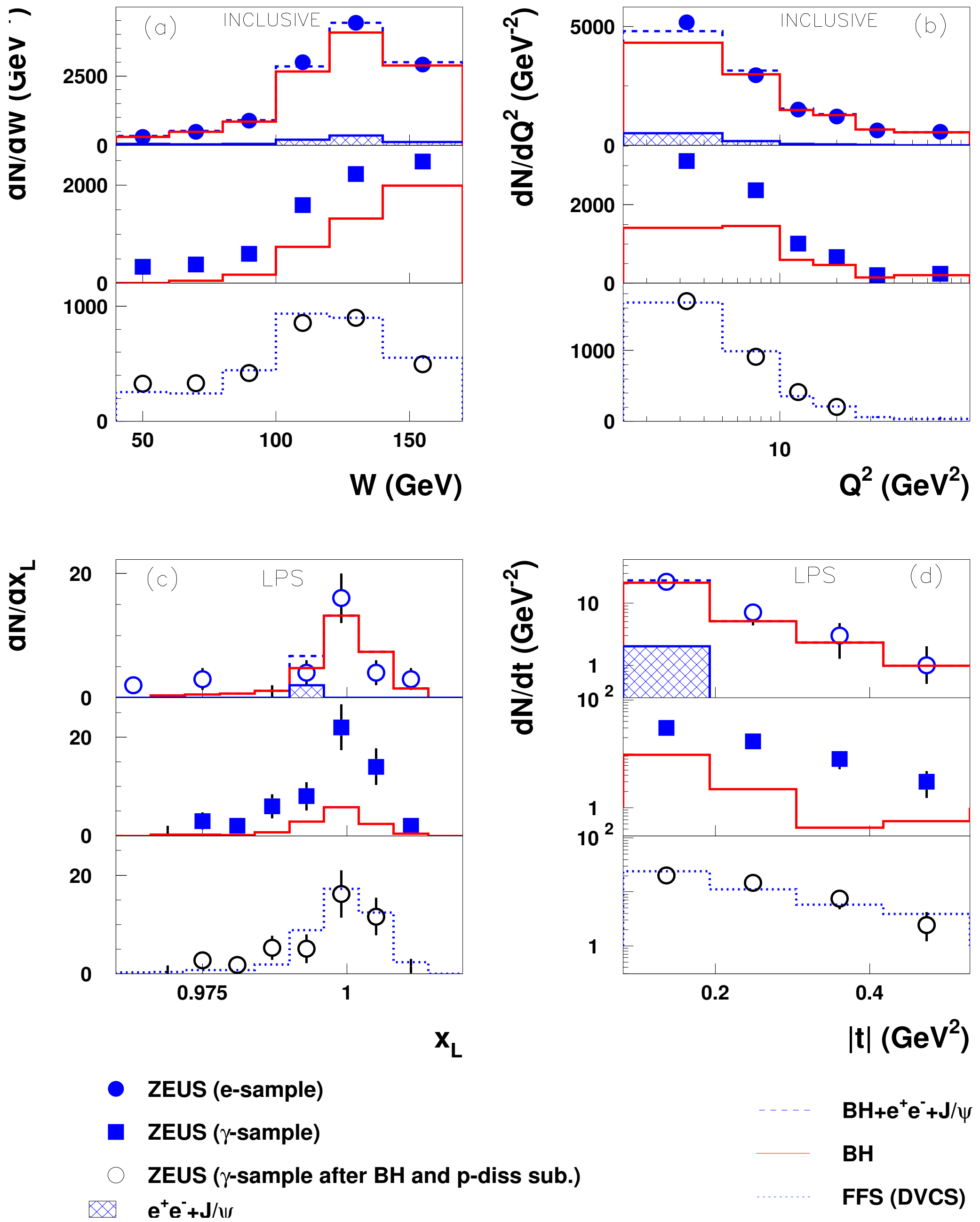

Figure 1: *Distribution of (a) W, (b) Q^2 in the inclusive sample and of (c) x_L and (d) $|t|$ in the LPS data sample, for the e-sample (top), the γ-sample (middle) and the γ-sample after BH background and proton dissociation subtraction (bottom). Also shown are the expectations of the MC normalised to the luminosity of the data and the contribution from exclusive dilepton production (e^+e^-), as depicted in the figure.*

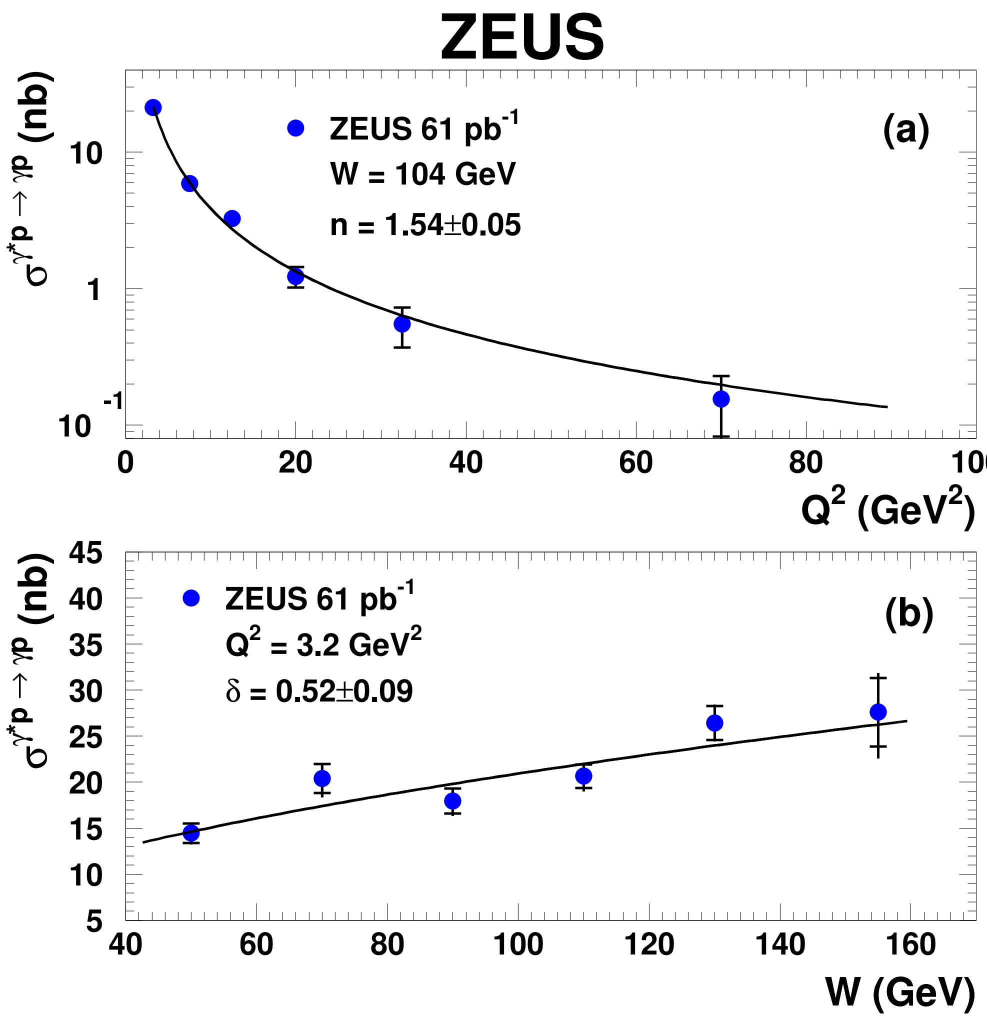

Figure 2: *(a) The DVCS cross section, $\sigma^{\gamma^* p \to \gamma p}$, as a function of Q^2. The solid line is the result of a fit of the form $\sim Q^{-2n}$. (b) The DVCS cross section, $\sigma^{\gamma^* p \to \gamma p}$, as a function of W. The solid line is the result of a fit of the form $\sim W^{\delta}$. The inner error bars represent the statistical uncertainty while the outer error bars the statistical and systematic uncertainties added in quadrature.*

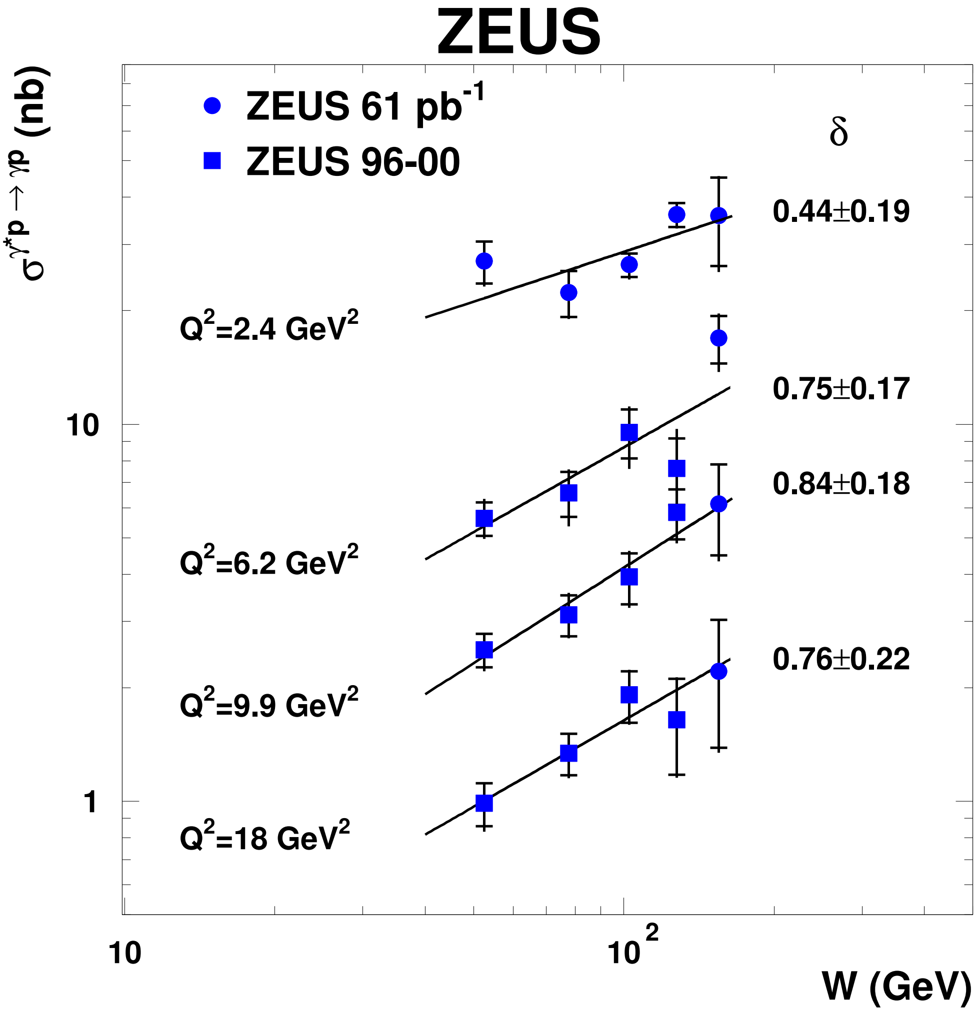

Figure 3: *The DVCS cross section, $\sigma^{\gamma^* p \to \gamma p}$, as a function of W for $Q^2 = 2.4$ GeV^2 (dots) shown together with previous ZEUS measurements (squares). Also shown at higher Q^2 are the new measurements at $W = 155$ GeV (dots). The solid lines are the results of a fit of the form $\sigma^{\gamma^* p \to \gamma p} \propto W^\delta$. The values of δ and their statistical uncertainties are given in the figure. The inner error bars represent the statistical uncertainty while the outer error bars the statistical and systematic uncertainties added in quadrature.*

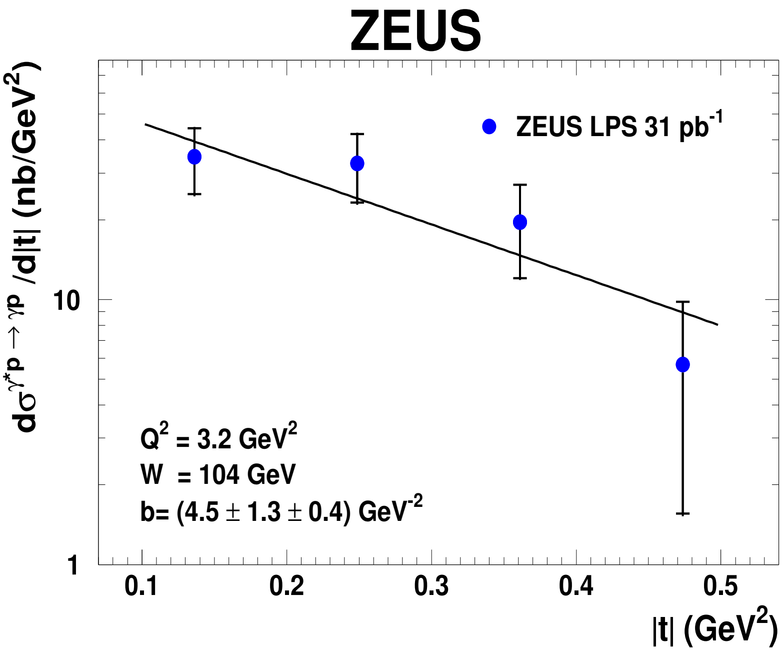

Figure 4: *The DVCS differential cross section, $d\sigma^{\gamma^* p \to \gamma p}/dt$, as a function of $|t|$. The solid line is the result of a fit of the form $\sim e^{-bt}$. The inner error bars represent the statistical uncertainty while the outer error bars the statistical and systematic uncertainties added in quadrature.*

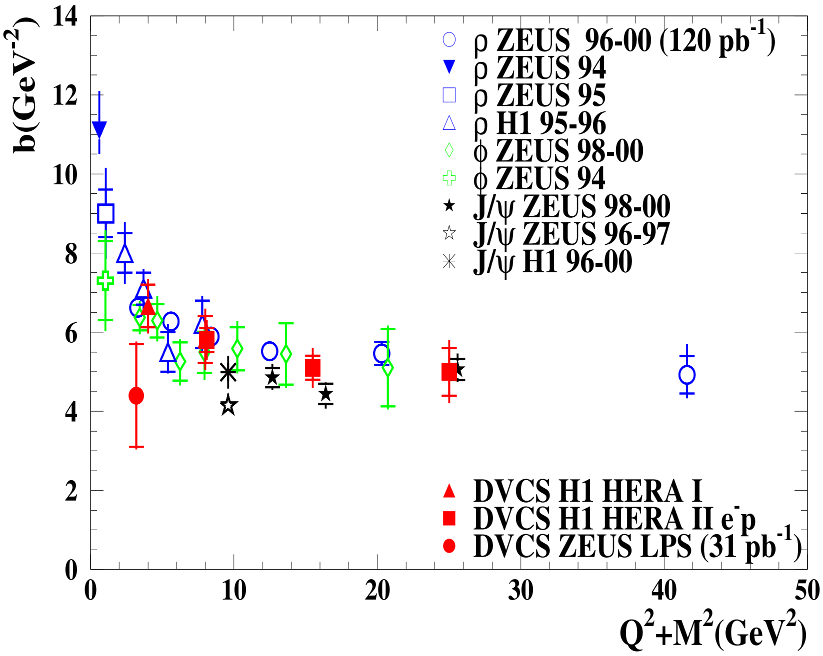

Figure 5: *A compilation of the values of the slope b as a function of $Q^2 + M^2$ for various exclusive processes including the present DVCS measurement. The inner error bars represent the statistical uncertainty while the outer error bars the statistical and systematic uncertainties added in quadrature.*